Magneto-optics of layers of double quantum dot molecules

L. M. Thu and O. Voskoboynikov*
Department of Electronic Engineering and Institute of Electronics, National Chiao Tung University, Hsinchu 30050, Taiwan
(Received 20 March 2009; revised manuscript received 18 August 2009; published 20 October 2009)

We present a general treatment of the magneto-optical response from systems of semiconductor nano objects of arbitrary shapes. Our theoretical hybrid method allows us to simulate the coherent manipulation of the quantum states of electrons and holes in nano objects and monitor that by means of analysis of the collective magneto-optical response from the system. As an example of the method implementation we consider the coherent manipulation of the electronic states of a asymmetrical double InAs quantum dot molecule embedded in GaAs matrix and the collective magneto-optical properties of a layer of the molecules. Our simulation results show that changes in the quantum-mechanical configuration of the quantum dot molecules can be observable by monitoring changes in the ellipsometric data obtained for layers made from these nano objects. The ellipsometric data clearly represent the quantum mechanics of the molecules.

DOI: 10.1103/PhysRevB.80.155442 PACS number(s): 73.21.−b, 75.20.Ck, 75.75.+a, 78.20.Bh

I. INTRODUCTION

Semiconductor nanostructured metamaterials potentially can manipulate electromagnetic fields in the optical range. The smallest building blocks of these metamaterials are made from direct-gap semiconductor's nano objects, such as quantum dots and quantum dot molecules. At the same time those objects are expected to play an important role in development of new physics and various applications in photonics as well as in electronics and solid-state quantum memory.[1,2] Progress in modern semiconductor technologies has allowed us to experimentally and theoretically model the various semiconductor nanostructures within a wide range of geometries and material parameters. For instance, it is possible to fabricate vertically stacked quantum dots [quantum dot molecules (QDMs)] of high quality and uniformity.[3–5] The quantum-mechanical coherent coupling and forming of molecular states in the stacked quantum dots can be considered in complete analogy to real molecules. But in contrast to the real molecules the artificial design of semiconductor QDMs provides us with the unique opportunity to dynamically manipulate and reconfigure wave functions of electrons and holes confined in QDM (see, for instance, Refs. 6–15 and references therein). QDMs have attracted much interest because they are very likeable candidates for the implementation of quantum bits.[2] From the other side, proper understanding of the connection between the electronic-state coherent coupling in isolated nano objects and the collective electromagnetic response of layers assembled from them[16] is a prerequisite to make new nanostructured metamaterials, with on-demand properties not resembling anything in nature.[17–23] We should conclude that the future development of the quantum informatics and metamaterial's quantum optics both require for an extensive investigation of the collective response of ensembles of semiconductor QDMs.

In order to reach those goals in this theoretical study we formulate a computational method which allows us to monitor the coherent manipulation of the quantum states of electrons and holes in embedded semiconductor nano objects by means of the magnetoellipsometry. The influence of the surrounding semiconducting matrix on the polarizability of the nano objects has been imposed using a generalization of the hybrid discrete-continuum model.[16,24,25] The generalization allows us to simulate the nano objects of arbitrary shapes. We show that parameters of the electron and hole quantum states localized in the nano objects can be retrieved from the collective magneto-optical response of systems of such nano objects. As an example of the method implementation we consider impact of the coherent manipulation of electronic states in the double vertical lens-shaped circular QDM on the collective magneto-optical response from a layer of those nano objects. The manipulation is performed by an external magnetic field applied upon InAs/GaAs quantum dot molecules assembled from the dots with substantially different lateral radii. Recently it was demonstrated that in the asymmetrical QDM the nonuniform diamagnetic shifts of the lowest electron-energy levels lead to their anticrossing which yields in a positive peak of the differential magnetic susceptibility of the system.[26] In this paper we show unusual consequences of the nonuniform diamagnetic shifts for the magneto-optics of layers of asymmetrical QDMs. We treat the semiconductor QDMs within complete three-dimensional description which allows us to simulate arbitrary directions of the external magnetic field (Fig. 1.) in contrast to most of the calculations done before. It brings up much wider opportunities to dynamically manipulate electron and hole states in QDMs. As it was already mentioned changes in magneto-

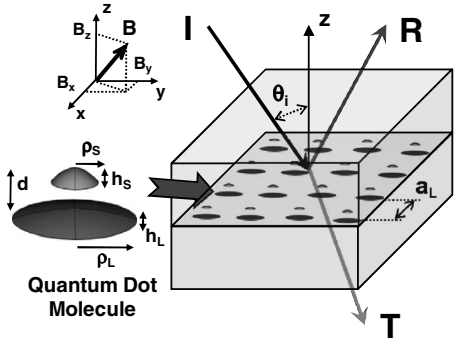

FIG. 1. Schematic of the magneto-optics of a layer of embedded semiconductor quantum dot molecules.

optical response of a layer of QDMs emerge from the changes in the quantum-mechanical configuration of the QDMs. In this paper we demonstrate in detail that the magnetoellipsometric data can reproduce an important and clear information on the quantum mechanics of the molecules.

II. THEORY

A. Hybrid model and discrete dipole approximation

In order to make this paper more self-contained, we will repeat and reformulate some of the aspects of the theory presented in Refs. 16, 24, and 25. We consider a system (layer) of QDMs of characteristic size a embedded into a semiconductor host matrix, which is transparent for the incoming (external) light beam (Fig. 1). For such a system we assume $\lambda \gg a_L > a$, where λ is the wavelength of the electromagnetic wave and a_L is an average distance between QDMs. It has been shown in Ref. 24 that under those assumptions we can use the hybrid model to describe the optical response of the system by means of polarizabilities of discrete dipoles embedded into the continues dielectric matrix. All the dipoles are assigned to the xy plane. The incoming light beam has a simple plane-wave character

$$\mathbf{E}_X(\mathbf{r}) = \mathbf{E}_0 e^{i\mathbf{k}_m \mathbf{r}},$$

$$\mathbf{k}_m = \sqrt{\epsilon_m}\mathbf{k}, \tag{1}$$

$$\mathbf{k} = (k_\parallel, k_z) = (k_x, k_y, k_z), \tag{2}$$

where ϵ_m stands for the dielectric constant of the host matrix, $k = \omega/c$ is the vacuum wave vector, and ω represents the light frequency.

In the linear discrete dipole approximation (DDA) (see Refs. 27 and 28, and references therein) the QDM's excess dipole strength $\mathbf{p}$ follows from Ref. 24

$$\mathbf{p} = \int_{\mathrm{QDM}} d\mathbf{r}^3 [\mathbf{P}(\mathbf{r}) - \mathbf{P}_m(\mathbf{r})], \tag{3}$$

where $\mathbf{P}(\mathbf{r})$ is the polarization density inside the QDM with the dielectric constant ϵ_{QDM} and $\mathbf{P}_m(\mathbf{r})$ is one of the host matrix with the dielectric constant ϵ_m. The embedded bare polarizability $\overleftrightarrow{\alpha}_{EB}$ is defined with respect to the internal applied electric field $\mathbf{E}_A$ [a spatial average of the internal to the QDM microscopic electric field $\mathbf{e}(\mathbf{r})$] by

$$\mathbf{p} = \overleftrightarrow{\alpha}_{EB} \mathbf{E}_A. \tag{4}$$

Within the electromagnetic nonlocal discrete description

$$\mathbf{E}_A = \mathbf{E}_L + \overleftrightarrow{\mathbf{t}}\mathbf{p}, \tag{5}$$

where $\mathbf{E}_L$ is the classical local field, which is equal to the external plane-wave field $\mathbf{E}_X$ in the case of a single QDM, and $\overleftrightarrow{\mathbf{t}}$ is the full electromagnetic self-interaction tensor for the QDM. The bare polarizability can be obtained by means of theory.[16,29]

The embedded dressed polarizability $\overleftrightarrow{\alpha}_{ED}$ refers to experimental observations and it is defined by

$$\mathbf{p} = \overleftrightarrow{\alpha}_{ED} \mathbf{E}_L. \tag{6}$$

The elementary relationship between those two kinds of polarizability can be written as

$$\overleftrightarrow{\alpha}_{EB}^{-1} - \overleftrightarrow{\alpha}_{ED}^{-1} = \overleftrightarrow{\mathbf{t}}. \tag{7}$$

For our system of embedded QDMs in the linear DDA we can write the local field at the position $\mathbf{r}_i$ of the ith dipole as

$$\mathbf{E}_{Li} = \mathbf{E}_{Xi} + \frac{1}{\epsilon_m} \sum_{j \neq i} \overleftrightarrow{\mathbf{f}}_{ij} \mathbf{p}_j, \tag{8}$$

$$\mathbf{E}_{Xi} = \mathbf{E}_X(\mathbf{r}_i), \tag{9}$$

where $\overleftrightarrow{\mathbf{f}}_{ij}$ is the vacuum intercellular (interdipole) transfer tensor [the dyadic Green's function in the DDA(Ref. 27)]

$$\overleftrightarrow{\mathbf{f}}_{ij} = \overleftrightarrow{\mathbf{f}}(\mathbf{r}_i - \mathbf{r}_j) = \frac{\exp(ik_m \Delta r_{ij})}{4\pi\epsilon_0 \Delta r_{ij}} \times \left[k_m^2 (\overleftrightarrow{\mathbf{I}} - \Delta\hat{\mathbf{r}}_{ij} \Delta\hat{\mathbf{r}}_{ij}^T) - \frac{1 - ik_m \Delta r_{ij}}{\Delta r_{ij}^2} (\overleftrightarrow{\mathbf{I}} - 3\Delta\hat{\mathbf{r}}_{ij} \Delta\hat{\mathbf{r}}_{ij}^T) \right],$$

$$\Delta\mathbf{r}_{ij} = \mathbf{r}_i - \mathbf{r}_j, \quad \Delta\hat{\mathbf{r}}_{ij} = \frac{\Delta\mathbf{r}_{ij}}{\Delta r_{ij}}$$

and $\overleftrightarrow{\mathbf{I}}$ is the identity dyadic. The induction for the excess dipole strength's $\mathbf{p}_i$ becomes

$$\mathbf{p}_i = \overleftrightarrow{\alpha}_{EDi} \left(\mathbf{E}_{Xi} + \frac{1}{\epsilon_m} \sum_{j \neq i} \overleftrightarrow{\mathbf{f}}_{ij} \mathbf{p}_j \right). \tag{10}$$

From Eq. (10) we obtain the system of equations to be solved

$$\sum_j \overleftrightarrow{\mathbf{T}}_{ij} \mathbf{p}_j = \mathbf{E}_{Xi}, \tag{11}$$

where

$$\overleftrightarrow{\mathbf{T}}_{ij} = \delta_{ij} (\overleftrightarrow{\alpha}_{EBi}^{-1} - \overleftrightarrow{\mathbf{t}}_i) + (1 - \delta_{ij}) \overleftrightarrow{\mathbf{f}}_{ij},$$

$$\overleftrightarrow{\mathbf{t}}_i = \overleftrightarrow{\mathbf{t}}_i^S + \frac{i\omega^3}{6\pi\epsilon_m \epsilon_0^3} \overleftrightarrow{\mathbf{I}},$$

$\overleftrightarrow{\mathbf{t}}_i^S$ is the static part of the self-interaction tensor to which we have added the Lorentz radiation damping (the term with ω^3 above).

The collective optical response of the system is characterized by the reflection and transmission coefficients. They have to be obtained from the far-field expression of the remote dipole field at a point $\mathbf{r}$ far from the layer location. Using solutions of Eq. (11) we get, for the reflection and transmission, respectively,

$$\mathbf{E}_R(\mathbf{r}) = \sum_i \overleftrightarrow{\mathbf{F}}_i(\mathbf{r}) \mathbf{p}_i, \quad \text{when } z \to +\infty;$$

$$\mathbf{E}_T(\mathbf{r}) = \mathbf{E}_X(\mathbf{r}) + \sum_i \overleftrightarrow{\mathbf{F}}_i(\mathbf{r}) \mathbf{p}_i, \quad \text{when } z \to -\infty, \tag{12}$$

where

$$\vec{\mathbf{F}}_i(\mathbf{r}) = \frac{\exp(ik_m\Delta r_i)}{4\pi\epsilon_0\epsilon_m\Delta r_i}k_m^2(\vec{\mathbf{I}} - \Delta\hat{\mathbf{r}}_i\Delta\hat{\mathbf{r}}_i^T),$$

$$\Delta\mathbf{r}_i = \mathbf{r} - \mathbf{r}_i.$$

After Eq. (12) it is trivial to calculate the transmission and reflection coefficients of the layer. The formulation of the systems (11) and (12), in general, traces a method of simulation of the optical response from an arbitrary system of semiconductor nano objects embedded into semiconductor host materials. The larger the tensor matrix $\vec{\mathbf{T}}_{ij}$, the more interesting problems may be studied. But therefore (if we would like to consider three-dimensional random arrays of semiconductor nano objects) the calculation of the matrix elements of $\vec{\mathbf{T}}_{ij}$ required and solution of Eq. (11) are already tedious problems themselves. So, in this paper we confine ourselves to a single layer (two-dimensional array) of QDMs embedded the semiconductor host matrix (Fig. 1)

In the case of a two-dimensional square lattice of QDMs of the lattice parameter a_L the calculation of the optical response of the embedded layer can be performed on the base of the Vlieger's expression[30,31]

$$\mathbf{E}_R(\mathbf{r}) = \vec{\mathbf{F}}(\mathbf{r})\mathbf{p}_{ef}, \tag{13}$$

where

$$\vec{\mathbf{F}}(\mathbf{r}) = \frac{ik_m^2 e^{i\bar{\mathbf{k}}_m\mathbf{r}}}{2\epsilon_0\epsilon_m a_L^2 k_{mz}}(\vec{\mathbf{I}} - \Delta\hat{\bar{\mathbf{k}}}_m\Delta\hat{\bar{\mathbf{k}}}_m^T)$$

is the Vlieger's remote interplanar transfer tensor, $\bar{\mathbf{k}}_m = \mathbf{k}_\parallel - k_z\hat{\mathbf{z}}$ and the effective dipole $\mathbf{p}_{ef}$ induced in the layer is obtained from

$$\mathbf{p}_{ef} = [\vec{\mathbf{I}} - \vec{\boldsymbol{\alpha}}_{EB}\vec{\mathbf{f}}]^{-1}\vec{\boldsymbol{\alpha}}_{EB}\mathbf{E}_0,$$

$$\vec{\mathbf{f}} = \frac{\vec{\mathbf{f}}^S}{4\pi\epsilon_0\epsilon_m a_L^3} + \vec{\mathbf{t}}^S + \frac{i(k_m^2\vec{\mathbf{I}} - \Delta\mathbf{k}_{\parallel m}\Delta\mathbf{k}_{\parallel m}^T - k_{mz}^2\hat{\mathbf{z}}\hat{\mathbf{z}}^T)}{2\epsilon_0\epsilon_m a_L^2 k_{mz}}, \tag{14}$$

$$\mathbf{f}_{xx}^S = \mathbf{f}_{yy}^S = -\frac{\mathbf{f}_{zz}^S}{2} = -4.51681. \tag{15}$$

Using the Vlieger's approach we can determine the reflection (r_{ss}, r_{pp}) and transmission (t_{ss}, t_{pp}) coefficients, and absorbance (A_{ss}, A_{pp}) of the layer. For a two-dimensional array (square lattice) of the dipoles, the coefficients are given by[30,31]

$$r_{ss} = \frac{f}{A_y\cos\theta_i - f},$$

$$r_{pp} = \frac{f\cos\theta_i}{A_x - f\cos\theta_i} - \frac{f\sin^2\theta_i}{A_z\cos\theta_i - f\sin^2\theta_i},$$

$$t_{ss} = 1 + r_{ss},$$

$$t_{pp} = \frac{f\cos\theta_i}{A_x - f\cos\theta_i} - \frac{A_z\cos\theta_i}{A_z\cos\theta_i - f\sin^2\theta_i},$$

$$A_{ss(pp)} = 1 - |r_{ss(pp)}|^2 - |t_{ss(pp)}|^2. \tag{16}$$

Here subscribers "s" and "p" refer to the light polarization perpendicular and parallel to the plane of incidence, respectively, θ_i is angle of incidence

$$A_\mu = 4\pi\epsilon_0 a_L^3(\alpha_{EB\mu\mu}^{-1} - t_{\mu\mu}) - \frac{\mathbf{f}_{\mu\mu}^S}{\epsilon_m},$$

$$f = 2\pi i a_L k_m.$$

The ellipsometric angles Ψ and Δ represent the experimental values and can be measured with the highest accuracy. They follow from a conventional definition

$$\frac{r_{pp}}{r_{ss}} = \tan\Psi e^{i\Delta}$$

and also can be calculated numerically.

B. Polarizability and quantum mechanics of QDMs

The hybrid discrete-continuum method allows us to simulate the collective electromagnetic response of the layer of embedded QDMs.[24,25] The embedded bare polarizability $\vec{\boldsymbol{\alpha}}_{EB}$ of a single QDM approximated at the near resonance conditions can be written as[16,22,24,29,32–34]

$$\vec{\boldsymbol{\alpha}}_{EB}(\omega) = \vec{\boldsymbol{\alpha}}_{EB}^S + \vec{\boldsymbol{\alpha}}^D(\omega), \tag{17}$$

where $\vec{\boldsymbol{\alpha}}_{EB}^S$ is the static part of the polarizability[35,36] of the QDM (to be treated later) and

$$\vec{\boldsymbol{\alpha}}^D(\omega) = \frac{e^2}{\hbar}\sum_n \mathbf{r}_n^*\mathbf{r}_n^T f_n(\omega) \tag{18}$$

is the dynamic part of the polarizability. In the equations above: $\mathbf{r}_n$ stands for the optical transition-matrix element[16,29,37]

$$f_n(\omega) = \left(\frac{E_n}{\hbar\omega}\right)\left[\frac{1}{\omega_n - \omega - i\Gamma_n}\right] \tag{19}$$

is the frequency-dependent function introduced in Refs. 16 and 29, which depends on transition energies $E_n = \hbar\omega_n$ of the resonance optical transitions of the QDM and corresponding damping factors Γ_n, e is the elementary charge. Faraday/Kerr or Cotton/Mouton-type magneto-optical effects are not taken into account here.

To find the static part of the polarizability tensor $\vec{\boldsymbol{\alpha}}_{EB}^S$ we implement the following boundary-value problem for a local electrostatic potential $\Phi(\mathbf{r})$ in a complex three-dimensional cubic domain of the host material including one QDM (Refs. 35 and 36)

$$\nabla_{\mathbf{r}}[\epsilon(\mathbf{r})\nabla_{\mathbf{r}}\Phi(\mathbf{r})] = 0,$$

$$-L < \mu < L, \quad \mu = \{x, y, z\}, \tag{20}$$

where

$$\epsilon(\mathbf{r}) = \begin{cases} \epsilon_{\mathrm{QDM}}, & \text{when } \mathbf{r} \text{ is inside QDM} \\ \epsilon_m, & \text{when } \mathbf{r} \text{ is outside QDM} \end{cases}.$$

An isolated QDM is located in the center of the domain and $L \gg a$. We solve the problem (20) in conjunction with three sets of the boundary conditions

$$s_x \begin{cases} \Phi(\mathbf{r})|_{-L,y,z} = \Phi(\mathbf{r})|_{x,\pm L,z} = \Phi(\mathbf{r})|_{x,y,\pm L} = 0 \\ \Phi(\mathbf{r})|_{+L,y,z} = 2LE_0 \end{cases},$$

$$s_y \begin{cases} \Phi(\mathbf{r})|_{x,-L,z} = \Phi(\mathbf{r})|_{\pm L,y,,z} = \Phi(\mathbf{r})|_{x,y,\pm L} = 0 \\ \Phi(\mathbf{r})|_{x,+L,z} = 2LE_0 \end{cases},$$

$$s_z \begin{cases} \Phi(\mathbf{r})|_{x,y,-L} = \Phi(\mathbf{r})|_{\pm L,y,z} = \Phi(\mathbf{r})|_{x,\pm L,z} = 0 \\ \Phi(\mathbf{r})|_{x,y,+L} = 2LE_0 \end{cases}. \quad (21)$$

The solutions give us the space distribution of the electric field $\mathbf{E}(\mathbf{r}) = -\boldsymbol{\nabla}\Phi(\mathbf{r})$ and polarization density $\mathbf{P}(\mathbf{r}) = \epsilon_0[\epsilon(\mathbf{r}) - 1]\mathbf{E}(\mathbf{r})$ when the external uniform electric field $\mathbf{E}_0$ is parallel to $\hat{\mathbf{x}}$, $\hat{\mathbf{y}}$, or $\hat{\mathbf{z}}$ correspondingly. Following the scheme described above the static parts of the embedded bare polarizability, embedded dressed polarizability, and self-interaction tensor can easily be obtained according to Eqs. (4), (6), and (7) for the appropriate s_μ

$$\alpha^S_{EB\mu\mu} = \frac{d_\mu}{\tilde{E}_\mu},$$

$$\alpha^S_{ED\mu\mu} = \frac{d_\mu}{E_{0\mu}},$$

$$t^S_{\mu\mu} = (\alpha^S_{EB\mu\mu})^{-1} - (\alpha^S_{ED\mu\mu})^{-1}, \quad (22)$$

where

$$\tilde{\mathbf{E}} = \frac{1}{V}\int_{\mathrm{QDM}} d\mathbf{r}^3 \mathbf{E}(\mathbf{r})$$

and V is the QDM volume.

For the dynamic part of the polarizability we have to compute the transition energies and wave functions of electrons and holes confined in the asymmetrical InAs/GaAs QDM. In our calculations we use a three-dimensional hard-wall confinement potential and realistic semiconductor material parameters (for instance, the band offset of the InAs/GaAs strained heterostructure, corrected to the strain conditions band parameters, etc.). The electron states are described by means of the effective one-band Hamiltonian,[16,38,39] which can properly describe the strong nonparabolicity in the InAs conduction band[39–41]

$$\hat{\mathbf{H}}_e = \left[\hat{\boldsymbol{\Pi}}_{\mathbf{e}} \frac{1}{2m_e(E,\mathbf{r})} \hat{\boldsymbol{\Pi}}_{\mathbf{e}} + V_e(\mathbf{r})\right]\mathbf{I}_2 + \frac{\mu_B}{2} g_e(E,\mathbf{r})\boldsymbol{\sigma}\cdot\mathbf{B}, \quad (23)$$

where: $\mathbf{I}_2$ is the identity matrix of size 2, $\hat{\boldsymbol{\Pi}}_{\mathbf{e}} = -i\hbar\nabla_{\mathbf{r}} + e\mathbf{A}(\mathbf{r})$ is the momentum operator for electrons, $\nabla_{\mathbf{r}}$ is the spatial gradient, $\mathbf{A}(\mathbf{r}) = \frac{1}{2}(\mathbf{B}\times\mathbf{r})$ is the vector potential for the uniform arbitrary directed magnetic field $\mathbf{B} = (B_x, B_y, B_z)$, $m_e(E,\mathbf{r})$ is the energy and position-dependent electron effective mass

$$\frac{1}{m_e(E,\mathbf{r})} = \frac{2P^2}{3\hbar^2}\left[\frac{1}{E + E_g(\mathbf{r}) - V(\mathbf{r})} + \frac{1}{E + E_g(\mathbf{r}) - V(\mathbf{r}) + 2\Delta(\mathbf{r})}\right] \quad (24)$$

and

$$g_e(E,\mathbf{r}) = 2\left\{1 - \frac{m_0}{m_e(E,\mathbf{r})}\frac{\Delta(\mathbf{r})}{3[E + E_g(\mathbf{r})] + 2\Delta(\mathbf{r})}\right\} \quad (25)$$

is the electronic Landé factor. In the equations above: $E_g(\mathbf{r})$ and $\Delta(\mathbf{r})$ stand for the position-dependent band gap and spin-orbit splitting in the valence band, P is the momentum matrix element,[38,42] $\boldsymbol{\sigma}$ is the vector of the Pauli matrices, μ_B is the Bohr magneton, m_0 is the free-electron mass, and $V_e(\mathbf{r})$ is the hard-wall confinement potential for electron

$$V_e(\mathbf{r}) = \begin{cases} 0, & \text{when } \mathbf{r} \text{ is inside QDM} \\ V_e^0, & \text{when } \mathbf{r} \text{ is outside QDM} \end{cases}, \quad (26)$$

where V_e^0 is the conduction-band offset in the InAs/GaAs quantum dot.

For the proper description of the valence-band (hole) states in InAs/GaAs quantum dots we should consider multiband $\mathbf{k}\cdot\mathbf{p}$ Hamiltonian that allow for valence subband mixing (see, for instance, Refs. 14 and 43–46). For the transition frequencies being almost at the edge of the gap of the QDM material the heavy-light hole mixing should be included and the low-energy hole states can be described by the four-band Luttinger-Kohn Hamiltonian[14,40,41,46,47]

$$\hat{\mathbf{H}}_h = \frac{1}{2m_0}\begin{pmatrix} \hat{P}_+ & \hat{R} & -\hat{S} & 0 \\ \hat{R}^* & \hat{P}_- & 0 & \hat{S} \\ -\hat{S}^* & 0 & \hat{P}_- & \hat{R} \\ 0 & \hat{S}^* & \hat{R}^* & \hat{P}_+ \end{pmatrix} + V_h(\mathbf{r})\mathbf{I}_4, \quad (27)$$

where

$$\hat{P}_\pm = [(\gamma_1 \pm \gamma_2)\hat{\Pi}^2_{h\perp} + (\gamma_1 \mp 2\gamma_2)\hat{\Pi}^2_{hz}],$$

$$\hat{R} = -\sqrt{3}\gamma_2\hat{\Pi}^2_{h-},$$

$$\hat{S} = 2\sqrt{3}\gamma_3\hat{\Pi}_{h-}\hat{\Pi}_{hz}.$$

In the above expressions: $\mathbf{I}_4$ is the identity matrix of size 4, $\{\gamma_1, \gamma_2, \gamma_3\}$ is a set of the Luttinger parameters, the momentum operators $\hat{\boldsymbol{\Pi}}_h$ are defined as the following:

$$\hat{\boldsymbol{\Pi}}_h = -i\hbar\nabla_{\mathbf{r}} - e\mathbf{A}(\mathbf{r}),$$

$$\hat{\Pi}^2_{h\perp} = \hat{\Pi}^2_{hx} + \hat{\Pi}^2_{hy},$$

$$\hat{\Pi}_{h\pm} = \hat{\Pi}_{hx} \pm i\hat{\Pi}_{hy}$$

and $V_h(\mathbf{r})$ is the hard-wall confinement potential for holes

$$V_h(\mathbf{r}) = \begin{cases} 0, & \text{when } \mathbf{r} \text{ is inside QDM} \\ V_h^0, & \text{when } \mathbf{r} \text{ is outside QDM} \end{cases}, \quad (28)$$

where V_h^0 is the valence-band offset in the InAs/GaAs quantum dot.

For an electronic state confined in the QDM the wave function is presented by the two component spinor

$$\mathbf{F}_{el\sigma}^{\{2\}}(\mathbf{r}) = \begin{Bmatrix} F_{el}^{\uparrow}(\mathbf{r})|S\rangle|\uparrow\rangle \\ F_{el}^{\downarrow}(\mathbf{r})|S\rangle|\downarrow\rangle \end{Bmatrix}, \quad (29)$$

where l stands for the main quantum number, $\sigma=\uparrow,\downarrow$ refers to the spin polarization and $|S\rangle$ is a spherically symmetric Bloch function.[41,42] The envelop wave functions $F_{el}^{\sigma}(\mathbf{r})$ should satisfy the Schrödinger equation

$$\hat{\mathbf{H}}_{e\sigma}\begin{Bmatrix} F_{el}^{\uparrow}(\mathbf{r}) \\ F_{el}^{\downarrow}(\mathbf{r}) \end{Bmatrix} = E_{el\sigma}\begin{Bmatrix} F_{el}^{\uparrow}(\mathbf{r}) \\ F_{el}^{\downarrow}(\mathbf{r}) \end{Bmatrix}. \quad (30)$$

A confined hole state with the main quantum number k can be written as a four-component Luttinger spinor[14,42,47]

$$\mathbf{F}_{hkJ}^{\{4\}}(\mathbf{r}) = \begin{Bmatrix} F_{hk}^{+3/2}(\mathbf{r})\left|\frac{3}{2},+\frac{3}{2}\right\rangle \\ F_{hk}^{-1/2}(\mathbf{r})\left|\frac{3}{2},-\frac{1}{2}\right\rangle \\ F_{hk}^{+1/2}(\mathbf{r})\left|\frac{3}{2},+\frac{1}{2}\right\rangle \\ F_{hk}^{-3/2}(\mathbf{r})\left|\frac{3}{2},-\frac{3}{2}\right\rangle \end{Bmatrix}, \quad (31)$$

where $\{|\frac{3}{2},+\frac{3}{2}\rangle,|\frac{3}{2},-\frac{1}{2}\rangle,|\frac{3}{2},+\frac{1}{2}\rangle,|\frac{3}{2},-\frac{3}{2}\rangle\}$ is the conventional Luttinger-Kohn basis.[16,41,42,47] The envelop functions $F_{hk}^{J_z}(\mathbf{r})$ are the components of the hole's eigenfunction of the Hamiltonian (27)

$$\hat{\mathbf{H}}_h\begin{Bmatrix} F_{hk}^{+3/2,\nu}(\mathbf{r}) \\ F_{hk}^{-1/2,\nu}(\mathbf{r}) \\ F_{hk}^{+1/2,\nu}(\mathbf{r}) \\ F_{hk}^{-3/2,\nu}(\mathbf{r}) \end{Bmatrix} = E_{hk\nu}\begin{Bmatrix} F_{hk}^{+3/2,\nu}(\mathbf{r}) \\ F_{hk}^{-1/2,\nu}(\mathbf{r}) \\ F_{hk}^{+1/2,\nu}(\mathbf{r}) \\ F_{hk}^{-3/2,\nu}(\mathbf{r}) \end{Bmatrix}. \quad (32)$$

The above hole states are designated by the main quantum number k and their chirality $\upsilon=\Uparrow,\Downarrow$. The hole's chirality is isomorphic to the electronic spin-quantum number: states with opposite chirality are orthogonal and they are degenerate in the absence of magnetic field.[14,15,48,49] We use the computed electron and hole wave functions and energies to simulate the dynamic part of the polarizability tensor in Eq. (17).

III. NUMERICAL RESULTS AND DISCUSSION

Now we apply the strategy developed above to the case of a layer of double vertical lens-shaped circular quantum dot molecules. To do this we use realistic semiconductor material parameters and dimensions of the dots in the molecule known in literature.[15,42,45,50,51] Our molecule consists of two quantum dots with substantially different radii $\rho_L > \rho_S$ and heights $h_L < h_S$ (the subscripts L and S indicate "large" and "small" dots in Fig. 1). So, the QDM is nonuniform in z direction. All calculations were performed for the molecule with the following geometry parameters:[5,26] $\rho_L=25$ nm, $\rho_S=9.5$ nm, $h_L=3$ nm, $h_S=4$ nm, and a few interdot (base-to-base) distances d.

TABLE I. Components of the static parts of embedded polarizabilities $\vec{\vec{\alpha}}_{EB(D)}$ and self-interaction tensor $\vec{\vec{t}}$ of InAs/GaAs QDMs ($\alpha_0=4\pi\epsilon_0 a_L^3=11.127\times10^{-32}$ Fm^2).

	α_{EB}^S	α_{ED}^S	t^S
$\alpha_{xx(yy)}$	$5.167\times10^{-4}\alpha_0$	$5.119\times10^{-4}\alpha_0$	$-18.148\times\alpha_0^{-1}$
α_{zz}	$1.050\times10^{-4}\alpha_0$	$0.923\times10^{-4}\alpha_0$	$-1310.430\times\alpha_0^{-1}$

The static parts of the polarizability tensors of the QDM was calculated with the approach described above using COMSOL multiphysics package.[52] The dielectric constants are taken like the following: $\epsilon_{\text{QDM}}=\epsilon_{\text{InAs}}=15.2$ for the inside InAs material and $\varepsilon_m=\varepsilon_{\text{GaAs}}=13.1$ for the GaAs matrix. Note that due to the cylindrical symmetry of the QDM, the static parts of polarizability tensors are diagonal and $\alpha_{xx}^S=\alpha_{yy}^S \neq \alpha_{zz}^S$ (so, $t_{xx}^S=t_{yy}^S \neq t_{zz}^S$ as well). The corresponding normalized results for a system with the two-dimensional lattice parameter $a_L=100$ nm and interdot distance $d=10$ nm are given in Table I as an example. The results are used in our calculations of the magneto-optical response from the layer of QDMs.

In the first place we simulate the embedded bare polarizability $\vec{\vec{\alpha}}_{EB}(\omega)$ (and the magneto-optical response of the system) without excitonic effects (we ignore interaction between electrons and holes in optical transitions). Some excitonic effects in the QDMs are discussed in Appendix. For the noninteracting electrons and holes $\vec{\vec{\alpha}}^D(\omega)$ can be written as the following:[16,29]

$$\vec{\vec{\alpha}}^D(\omega) = \frac{e^2}{\hbar}\sum_{l,\sigma,J_z,k,\nu} \mathbf{r}_{e\sigma;J_z,h\nu}^{*}\mathbf{r}_{e\sigma;J_z,h\nu}^{T}|\langle F_{hk}^{J_z,\nu}|F_{el}^{\sigma}\rangle|^2 f_{k\nu,l\sigma}(\omega),$$

$$f_{k\nu,l\sigma}(\omega) = \left(\frac{E_{k\nu,l\sigma}}{\hbar\omega}\right)\left[\frac{1}{\omega_{k\nu,l\sigma}-\omega-i\Gamma_{k\nu,l\sigma}}\right], \quad (33)$$

where $\mathbf{r}_{eh}$ stands for the bulk interband optical matrix element,[16,37] $\hbar\omega_{k\nu,l\sigma}=E_{k\nu,l\sigma}=E_{hk\nu}+E_{el\sigma}+E_g$ present transition energies of the resonance optical transitions from hole energy levels $(hk\upsilon)$ to electron energy levels $(el\sigma)$ of the QDM, and $\Gamma_{k\nu,l\sigma}$ stand for the corresponding damping factors (E_g is the energy gap of the dot's semiconductor material). The hole-electron overlap integrals $\langle F_{hk}^{J_z,\nu}|F_{el}^{\sigma}\rangle$ should be calculated using the envelop functions $F_{el(hk)}^{\sigma(J_z,\nu)}$ from Eqs. (30) and (32).

To model the optical transition energies and overlap integrals we determine material parameters for the InAs/GaAs quantum dot molecule. According to the data from Refs. 14, 26, 44, 45, 50, and 51 we choose for the strained InAs inside the dot: $E_{g\text{InAs}}=0.842$ eV, $\Delta_{\text{InAs}}=0.39$ eV, $m_{e\text{InAs}}(0)=0.044\ m_0$, $\gamma_{1\text{InAs}}=11.65$, $\gamma_{2\text{InAs}}=3.86$, and $\gamma_{3\text{InAs}}=3.87$. For the GaAs surrounding matrix: $E_{g\text{GaAs}}=1.52$ eV, $\Delta_{\text{GaAs}}=0.341$ eV, $m_{e\text{GaAs}}(0)=0.067\ m_0$, $\gamma_{1\text{GaAs}}=6.98$, $\gamma_{2\text{GaAs}}$

=2.06, and γ_{3GaAs}=2.93. Using these parameters, the band offsets of conduction band and valence band can be found as: V_e^0=0.474 eV and V_h^0=0.203 eV. The energies and wave functions of electrons and holes confined in the QDM are obtained numerically form solutions of Eqs. (30) and (32) by the nonlinear iterative method[53] using the COMSOL multiphysics package.[52]

Now we present the transition energies and overlap integrals of noninteracting electrons and holes (excitonic effects are discussed in Appendix). We consider three distances between dots in the QDM: d_1=20 nm, d_2=10 nm, d_3=5 nm, and three directions of the magnetic field: $\mathbf{B}_{[1]}=(0,0,B\hat{\mathbf{z}})$, $\mathbf{B}_{[2]}=\frac{1}{\sqrt{2}}(0,B\hat{\mathbf{y}},B\hat{\mathbf{z}})$, $\mathbf{B}_{[3]}=(0,B\hat{\mathbf{y}},0)$. For the reason of clarity we concentrate on the optical transitions between four lowest hole energy states $h1(2)\nu$ ($\nu=\Uparrow,\Downarrow$) and four lowest electronic states $e1(2)\sigma$ ($\sigma=\uparrow,\downarrow$) under the condition of the spin-chirality alignment in the transition. In our general consideration the magnetic field is not parallel to the system growth direction $\hat{\mathbf{z}}$. This does not allow us to use any simple specific selection rules for the interband optical transitions. Now we should impose the following rule: certain transition is allowed when the corresponding three-dimensional overlap integral cannot be vanished.

For configurations $\{d_i,\mathbf{B}_{[j]}\}$ $(i,j=1,2,3)$ the lowest transition energies and corresponding overlap integrals are shown in Figs. 2–7. It should be noted that according to our simulation experience (see also Ref. 46) the predominant components of the Luttinger spinor $\mathbf{F}_{hkJ_z}^{\{4\}}$ are those of $J_z=\pm\frac{3}{2}$ for all involved hole states and the system's configurations. The components of $J_z=\pm\frac{1}{2}$ always give small corresponding contributions in this energy range. Therefore, for the optical transitions being considered $J_z=\pm\frac{3}{2}$ components

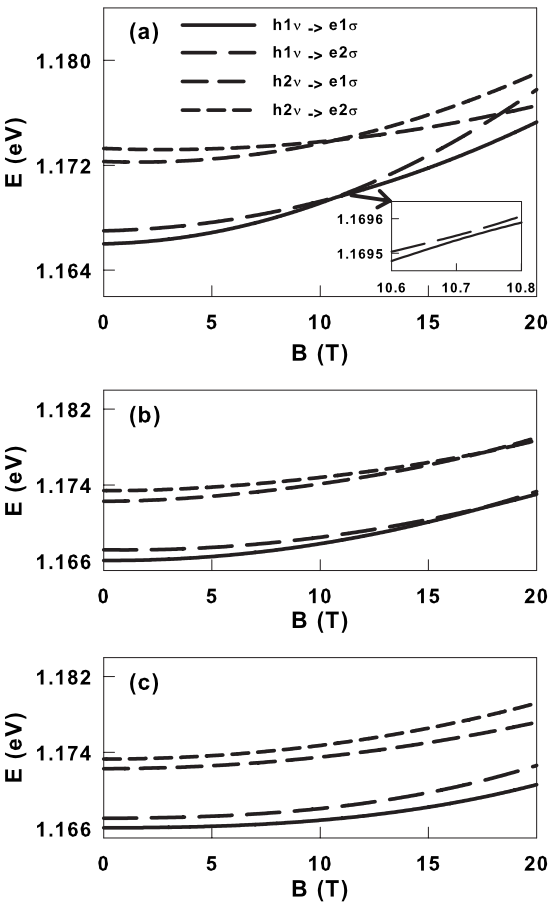

FIG. 2. Transition energies for $d=d_1$ as functions of magnetic field at different directions of the magnetic field. Inset: the anticrossing region.

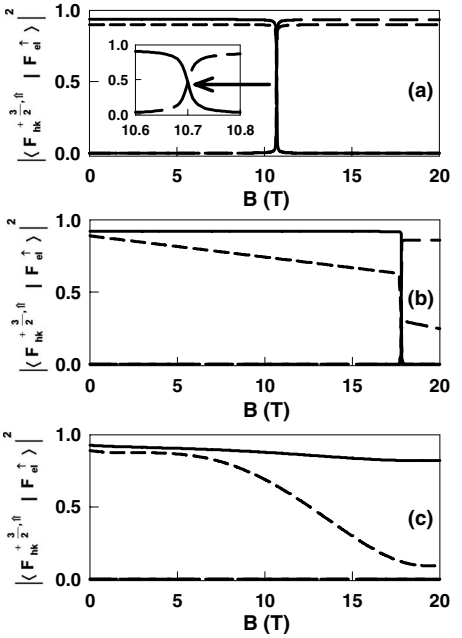

FIG. 3. Overlap integrals (squared absolute values) as functions of magnetic field for $d=d_1$ and different directions of the magnetic field [descriptions of the transitions see in Fig. 2(a)].

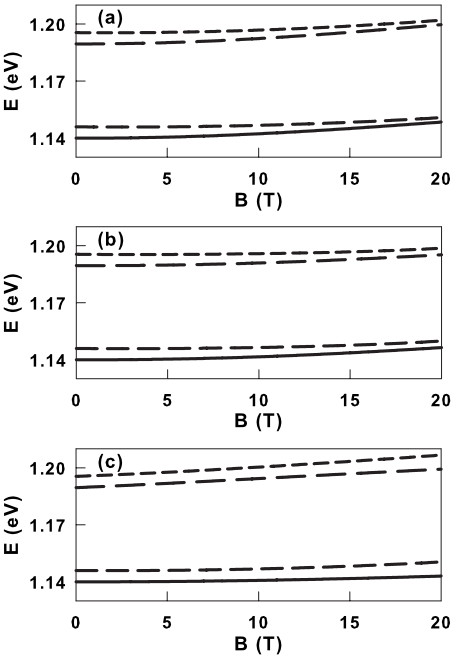

FIG. 4. Transition energies for $d=d_3$ as functions of magnetic field at different directions of the magnetic field [descriptions of the transitions see in Fig. 2(a)].

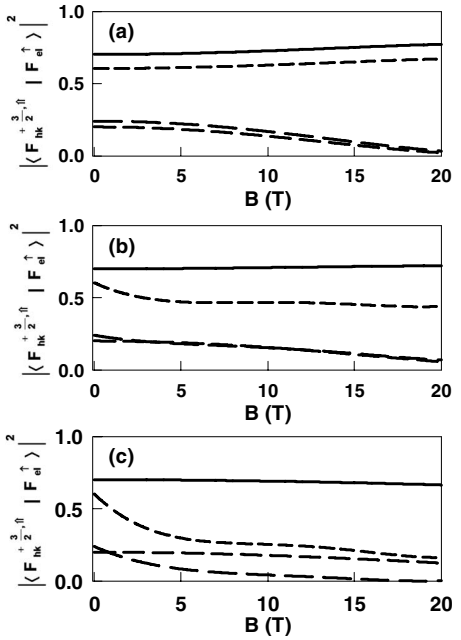

FIG. 5. Overlap integrals (squared absolute values) as functions of magnetic field for $d=d_3$ and different directions of the magnetic field [descriptions of the transitions see in Fig. 2(a)].

give the predominant (95%) contributions to the sum of the squared overlap integrals in the dynamic part of the polarizability [see Eq. (33)]. Using this result in Figs. 3, 5, and 7 we present only the squared absolute value of $\langle F_{hk}^{+3/2,\Uparrow}|F_{el}^{\uparrow}\rangle$.[54]

The first crucial difference between results for two distances d_1 and d_3 when $\mathbf{B}=\mathbf{B}_{[1]}$ is the anticrossing of the electronic energies. For the large distance between dots (d_1) the tunnel coupling between them is weak. The nonuniformity of the QDM geometry in z direction generates the nonuniform diamagnetic shifts of the electron energies[26] which leads to the anticrossing for $e1\sigma$ and $e2\sigma$ states at $B_{1AC} \approx 10.7$ T. The anticrossing was discovered and discussed in details in Ref. 26. At the same time energy levels for holes do not anticross within this range of the magnetic field. This leads to the anticrossing for the energies of $h1\nu \rightarrow e1\sigma$ and $h1\nu \rightarrow e2\sigma$ transitions [see inset of Fig. 2(a)]. Here we should stress that the anticrossing manifests redistribution of the electronic wave function inside the QDM: the electronic wave function of the state $e1\sigma$ at B_{1AC} relocates from the large dot to the small one. On the contrary, the second state $e2\sigma$ relocates from the small dot to the large one. At the same time, the probability density of the hole state $h1\nu$ remains to localize in the large dot and the probability density of the hole state $h2\nu$—in the small dot. This leads to the steplike behavior of the corresponding overlap integrals at $B=B_{1AC}$ [see Fig. 3(a)]. Clearly, when the distance between the dots in the QDM is large, the magnetic field can drastically change the overlap integrals for the corresponding optical transitions as it is shown in Fig. 3(a). The nonuniform diamagnetic shift also produces crossings between $h1\nu \rightarrow e2\sigma$ and $h2\nu \rightarrow e1\sigma$ transition energies at $B_{1C} \approx 18.3$ T [Fig. 2(a)]. But this crossing appears without relocations of the electron wave functions and it has no impact on the overlap integrals. The small distance (d_3) and strong tunnel coupling between dots lead to the strong hybridization between electronic states $e1\sigma$ and $e2\sigma$.[26,55] This creates molecular states for electrons with symmetric and antisymmetric configurations along z direction.[14,26,55] The diamagnetic shifts (when $\mathbf{B}=\mathbf{B}_{[1]}$) become uniform and no anticrossings (wave function's redistributions) or crossings appear [see Figs. 4(a) and 5(a)].

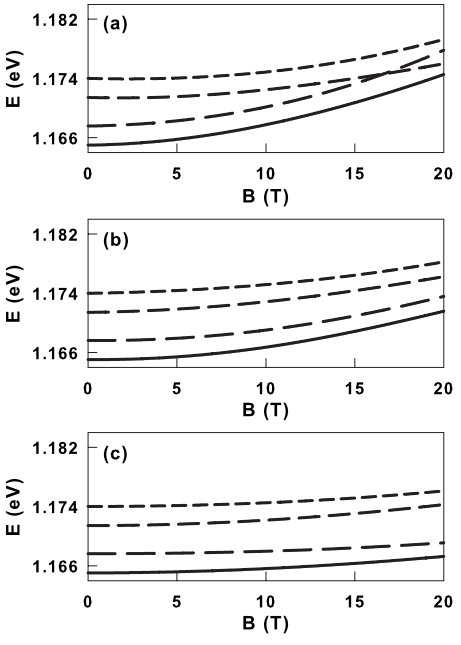

FIG. 6. Transition energies for $d=d_2$ as functions of magnetic field at different directions of the magnetic field [descriptions of the transitions see in Fig. 2(a)].

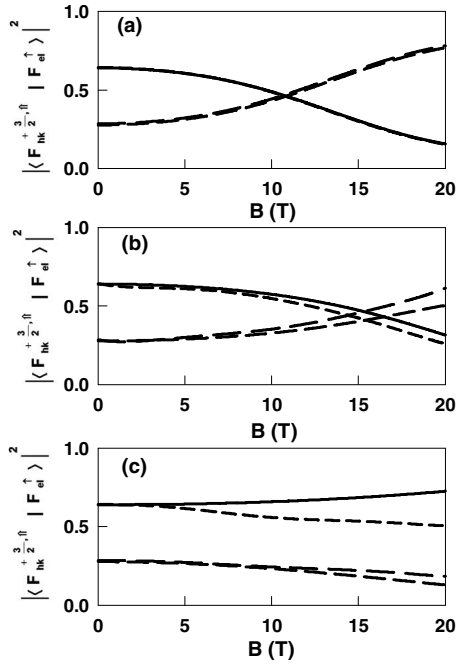

FIG. 7. Overlap integrals (squared absolute values) as functions of magnetic field for $d=d_2$ and different directions of the magnetic field [descriptions of the transitions see in Fig. 2(a)].

The system with the distance d_2 ($\mathbf{B}=\mathbf{B}_{[1]}$) presents an intermediate case when the anticrossing and hybridization coincide. This is the reason why a weak convergence of the energies for the transitions $h1\nu \rightarrow e1\sigma$ and $h1\nu \rightarrow e2\sigma$ and some typical changes in the overlap integrals can be seen in Figs. 6(a) and 7(a). Yet, the energy crossing for the transitions $h1\nu \rightarrow e2\sigma$ and $h2\nu \rightarrow e1\sigma$ remains at $B_{1C} \approx 16.6$ T.

To complete the picture of the interplay between of the distance and magnetic field impacts on the transition energies and overlap integrals, we show $E_{kl}(B)$ and $|\langle F_{hk}^{+3/2,\Uparrow}|F_{el}^{\uparrow}\rangle|^2$ for few directions of the magnetic field in Figs. 2–7. For the large distance between dots within the QDM (d_1) the change in the magnetic field direction from $\mathbf{B}_{[1]}$ to $\mathbf{B}_{[2]}$ leads to a shift of the anticrossing (crossing) point according to the obvious scaling rule [Fig. 2(b)]

$$B_{2AC} \approx \sqrt{2} B_{1AC},$$

$$B_{2C} \approx \sqrt{2} B_{1C}$$

[note: $B_{2C} \approx 25.9$ T and the crossing is located out of the range of Fig. 2(b)]. At the same time the overlap integrals at the anticrossing for the allowed transitions demonstrate some deviations from the pure steplike behavior. Figure 3(b) presents a typical manifestation of the changes in the electron and hole wave function's distributions between two dots. Again the decrease in the distance between dots removes the traces of the anticrossing and the wave function's relocation [Figs. 4(b), 5(b), 6(b), and 7(b)]. When the magnetic field is parallel to xy plane ($\mathbf{B}_{[3]}$ configuration) the anticrossing and crossing have disappeared even for $d=d_1$. The overlap integrals being functions on the magnitude of the magnetic field simply reflect changes in the confinement of the electron and hole wave functions along z direction in different dots. The electron states confined in high (small) dot are more sensitive to the magnetic field. The electron wave functions localized in the large dot are obviously under strong confinement in z direction already for $B=0$ and hardly can be squeezed more by the magnetic field applied along y direction. At the same time the sensitivity of the hole wave functions to the magnetic field is much weaker, no mater in which dot the function is localized. The reduction in the interdot distance conventionally hybridizes electron states from different dots. This finally forms a typical "molecular" magnetic properties of the QDM as it is shown in Figs. 4(c) and 5(c).

Using the above discussed quantum-mechanical properties of the transition energies and overlap integrals we investigate now the collective magneto-optical response of the layer of QDMs with the two-dimensional lattice parameter $a_L=100$ nm. First we combine all our data on the static parts of the polarizability tensors with the results of the quantum-mechanical calculations into the complete $\vec{\vec{\alpha}}_{EB}(\omega)$ using $r_{eh}=0.6$ nm.[16,37] Obviously, small damping parameter Γ ensures a clear reflection of the quantum-mechanical properties of an individual QDM in the collective magneto-optical response of the layer of QDMs. At the same time in our theory Γ has to be used as a free parameter.[16,29] To demonstrate importance of the parameter value we present in Fig. 8 the absorbance of the layer of the QDMs in $\{d_1;\mathbf{B}_{[1]}\}$ configuration for the incidence of $\theta_i=60°$. The inset of Fig. 8 gives a

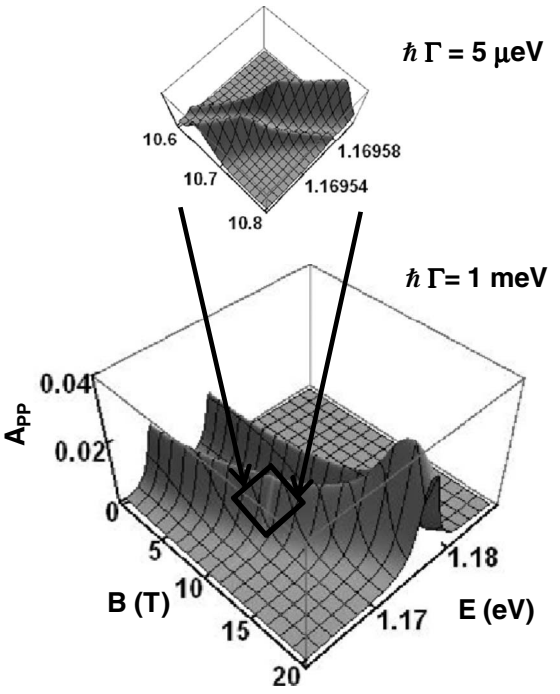

FIG. 8. Absorbance for a monolayer of InAs/GaAS QDMs in $\{d_1,\mathbf{B}_{[1]}\}$ configuration.

filling of the impact of the parameter on the observation of the energy gap at the anticrossing of the transition energies when Γ is small [see Inset of Fig. 2(a)]. The peak in Fig. 8 corresponds to the crossing of the two transition energies $h1\nu \rightarrow e2\sigma$ and $h2\nu \rightarrow e1\sigma$ in Fig. 2(a). In the crossing point they contribute in resonance simultaneously and this increases the response by the factor of 2. We should stress, that even for relatively large $\hbar\Gamma=1$ meV the quantum mechanics of the QDM clearly shows itself from the magneto-optical data. So, we will set $\hbar\Gamma=1$ meV for all calculations below. Note, we present here only peaks corresponding to the transitions considered in Figs. 2–7. Our calculation results show that we always can distinguish them if $\hbar\Gamma \leq 1$ meV.[16,24,25,55]

The ellipsometric angles Ψ and Δ can be measured with the highest accuracy. The direct accessibility of the quantum information from the QDMs such as individual dipole strengths, transition energies, and overlap integrals by means of the measurement of the ellipsometric parameters is one of the attractive aspects of our approach.

In order to illustrate that we show in Figs. 9–11 relevant data on the magnetoellipsometry of a layer of InAs/GaAs QDMs for the incidence of $\theta_i=60°$. For the ellipsometric angle Ψ the results systematically reproduce the transformation of the quantum-mechanical properties of the individual QDMs when we change the system configuration from $\{d_1,\mathbf{B}_{[1]}\}$ [Fig. 9(a)] to $\{d_3,\mathbf{B}_{[3]}\}$ [Fig. 11(f)]. The variation in the magnetic field magnitude makes the transformation even more clear and understandable. At the first glance the anticrossing features of the transition energies and overlap integrals are not clear in Figs. 9(a) and 9(b) for $\{d_1,\mathbf{B}_{[1]}\}$ configuration when $\hbar\Gamma=1$ meV (note, we can see them clearly if $\hbar\Gamma=1$ μeV). Yet, the crossing as another result of the nonuniform diamagnetic shift (pure quantum-mechanical

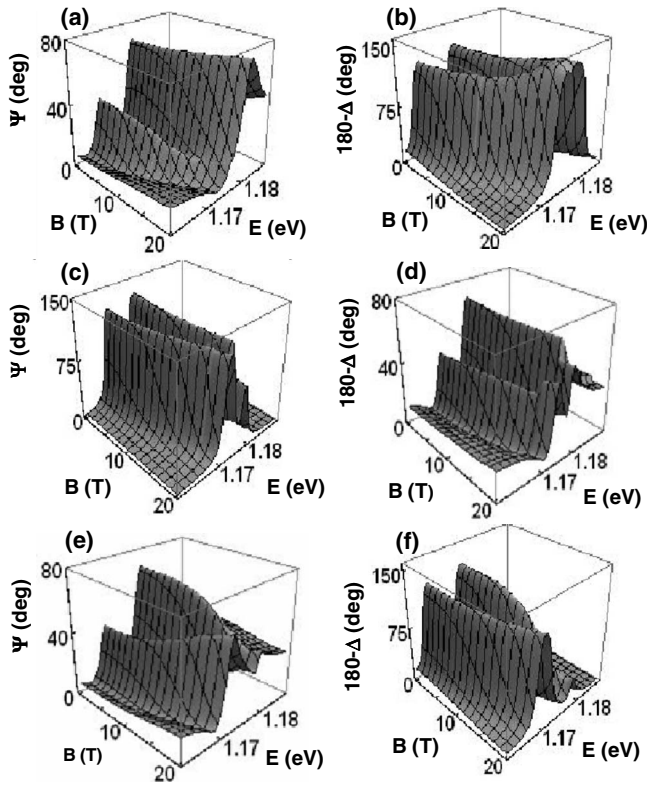

FIG. 9. Ellipsometric angles for $d=d_1$ and different directions of the magnetic field: [(a) and (b)]—$\mathbf{B}_{[1]}$; [(c) and (d)]—$\mathbf{B}_{[2]}$; and [(e) and (f)]—$\mathbf{B}_{[3]}$.

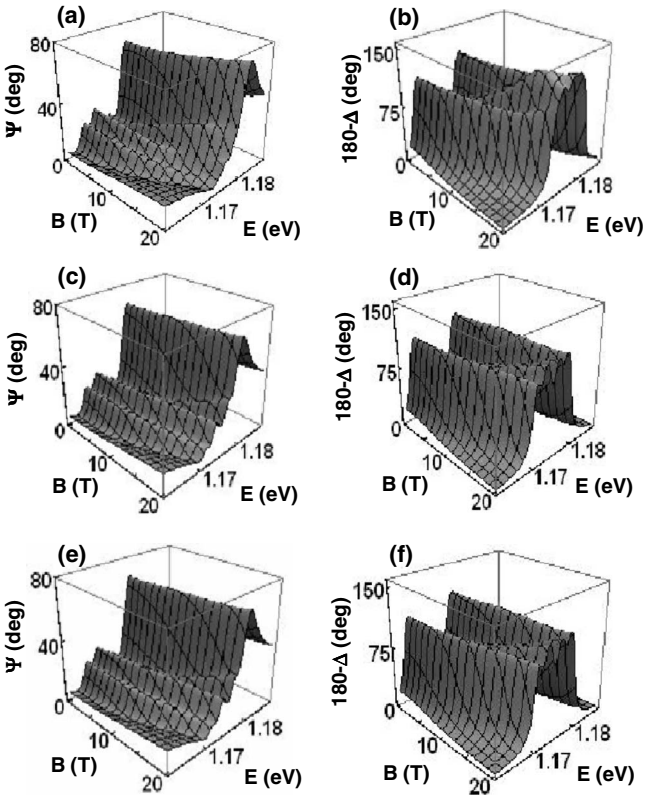

FIG. 10. Ellipsometric angles for $d=d_2$ and different directions of the magnetic field: [(a) and (b)]—$\mathbf{B}_{[1]}$; [(c) and (d)]—$\mathbf{B}_{[2]}$; and [(e) and (f)]—$\mathbf{B}_{[3]}$.

phenomenon) obviously shows itself as a combined peak in Figs. 9(b) and 10(b). In general the transformations of the overlap integrals (connected to the changes in electron wave-function localization) can be easily recognized in Figs. 9 and 10. Therefore we can say that, when the distance between dots in the QDM is large enough, the magnetic field acts as a dynamic coupling factor for electron energy states localized in different dots on the analogy of the interdot distance in the static approach. At the same time for the interdot distance d_3 the ellipsometry simply exhibits the conventional molecular diamagnetic shift for all directions of the magnetic field (Fig. 11). For all configurations the variation in both ellipsometric angles is clearly within the range of any modern ellipsometer[56] which gives us an opportunity to monitor optically coherent dynamic (when **B** is changing) and static (when d is changed) transformations and tuning of the electron wave functions in QDMs.

IV. CONCLUSION

For systems of semiconductor embedded nano objects of arbitrary shapes we have formulated a modification of the hybrid discrete dipole approximation. The modification allows us to describe the collective magneto-optical response of systems of such objects. As an example of the theory implementation we have performed a comparative study of the magneto-optical response functions (absorbance and the ellipsometric angles) for a layer of asymmetrical InAs quantum dot molecules arranged in a square two-dimensional lattice and embedded into GaAs matrix. The response of individual embedded QDMs is presented in terms of the excess polarizability. Static and dynamic parts of the polarizability (and the self-interaction tensor as well) are determined. Using the Veliger's derivation we simulated the ellipsometric angles of the layer embedded QDMs for a wide range of the system configuration. We emphasize that the magnetoellipsometric data reproduce important information on the quantum mechanics of the molecules. Varying magnetic field and the distance between quantum dots within the layer we can investigate optically the transition from molecular to "atomic" behavior of the system. This general conclusion remains valid when excitonic effects are taken into consideration. Our simulation results clearly suggest measurable values for the ellipsometric data for any modern ellipsometric setup. The approach can be potentially useful for simulation and characterization of new all-semiconductor nanostructured metamaterials.

ACKNOWLEDGMENTS

We thank Shao-Fu Xue for assistance in the calculations. O.V. thanks V. Ryzhii for his hospitality at the University of Aizu (Japan) where a part of the paper was written. This work is supported by the National Science Council of the Republic of China under Contracts No. NSC 97-2112-M-009-012-MY3, No. NSC 97-2120-M-009-004, and No. NSC 98-2918-I-009-001, and by the Ministry of Education of Tai-

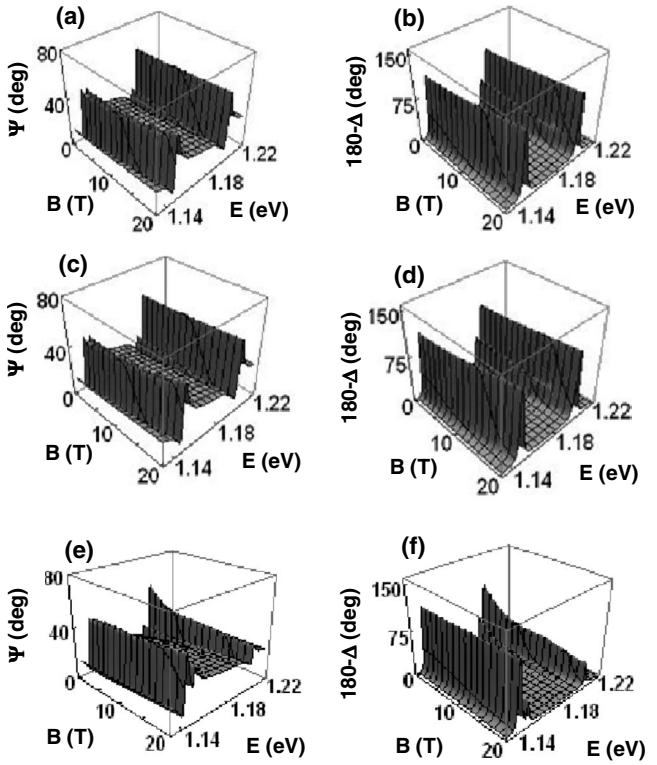

FIG. 11. Ellipsometric angles for $d=d_3$ and different directions of the magnetic field: [(a) and (b)]—$\mathbf{B}_{[1]}$; [(c) and (d)]—$\mathbf{B}_{[2]}$; and [(e) and (f)]—$\mathbf{B}_{[3]}$.

wan under Contract No. MOEATU 95W803.

APPENDIX

In this appendix we evaluate some impacts of the possible formation of the excitonic states in QDMs on the collective magneto-optical response of the layers of them. The excitonic Hamiltonian for QDM can be written as

$$\hat{\mathbf{H}}_{ex} = \hat{\mathbf{H}}_e + \hat{\mathbf{H}}_h - e^2 G(\mathbf{r}_e, \mathbf{r}_h), \tag{A1}$$

where $G(\mathbf{r}_e, \mathbf{r}_h)$ is the Green's function of the Poisson equation

$$\epsilon_0 \nabla_{\mathbf{r}} [\epsilon(\mathbf{r}) \nabla_{\mathbf{r}} G(\mathbf{r}, \mathbf{r}')] = -\delta(\mathbf{r} - \mathbf{r}'). \tag{A2}$$

The exciton wave function $\Psi_{ex}(\mathbf{r}_e, \mathbf{r}_h)$ can be expanded in terms of elements of the tensor product of two vector spaces: $\mathbf{\Lambda}_e(\mathbf{r}_e)$, which is spanned by $\mathbf{F}^{\{2\}}_{el\sigma}(\mathbf{r})$, when $\{F^{\uparrow}_{el}(\mathbf{r}_e), F^{\downarrow}_{el}(\mathbf{r}_e)\}$ are solutions of Eq. (30); and $\mathbf{\Lambda}_h(\mathbf{r}_h)$, which is spanned by $\mathbf{F}^{\{4\}}_{hkJ}(\mathbf{r})$, when $\{F^{+3/2,\nu}_{hk}(\mathbf{r}_h), F^{-1/2,\nu}_{hk}(\mathbf{r}_h), F^{+1/2,\nu}_{hk}(\mathbf{r}_h), F^{-3/2,\nu}_{hk}(\mathbf{r}_h)\}$ are solutions of Eq. (32) (Refs. 2, 44, 57, and 58)

$$\Psi_{ex}(\mathbf{r}_e, \mathbf{r}_h) = \sum_i a_i [\mathbf{\Lambda}_e(\mathbf{r}_e) \otimes \mathbf{\Lambda}_h(\mathbf{r}_h)]_i, \tag{A3}$$

where index i stands for a certain possible set of $\{el, \sigma; hk, \nu\}$ (a certain optical transition). We can obtain the excitonic transition energies E^n_{ex} from the secular equation

$$\det[(E_{el\sigma} + E_{hk\nu} + E_{g\mathrm{InAs}} - E_{ex})\delta_{ij} - e^2 G_{ij}] = 0 \tag{A4}$$

and define the coefficients a^n_i as solutions of the following system of linear equations:

$$\sum_j \{(E_{el\sigma} + E_{hk\nu} + E_{g\mathrm{InAs}})\delta_{ij} - e^2 G_{ij}\} a^n_j = E^n_{ex} a^n_i. \tag{A5}$$

In the equations above the matrix elements of the Green's function are given by

$$G_{ij} = \sum_{J_z, J'_z} \int F^{\sigma}_{el}(\mathbf{r}_e) F^{\sigma'}_{el'}(\mathbf{r}_e) V^{J_z,\nu;J'_z,\nu'}_{hk;hk'}(\mathbf{r}_e) d\mathbf{r}_e, \tag{A6}$$

where the summations run for $J_z(J'_z) = \pm\frac{3}{2}, \pm\frac{1}{2}$. In Eq. (A6)

$$V^{J_z,\nu;J'_z,\nu'}_{hk;hk'}(\mathbf{r}_e) = \int G(\mathbf{r}_e, \mathbf{r}_h) F^{J_z,\nu}_{hk}(\mathbf{r}_h) F^{J'_z,\nu'}_{hk'}(\mathbf{r}_h) d\mathbf{r}_h \tag{A7}$$

[according to Eq. (A2)] is a solution of the following equation:

$$\epsilon_0 \nabla_{\mathbf{r}} [\epsilon(\mathbf{r}) \nabla_{\mathbf{r}} V^{J_z,\nu;J'_z,\nu'}_{hk;hk'}(\mathbf{r})] = -F^{J_z,\nu}_{hk}(\mathbf{r}) F^{J'_z,\nu'}_{hk'}(\mathbf{r}). \tag{A8}$$

If the excitons contribute to the resonance optical transitions, ignoring quantum nonlocal effects[33] the dynamic part of the QDM polarizability can be written as

$$\overleftrightarrow{\boldsymbol{\alpha}}^D(\omega) = \overleftrightarrow{\boldsymbol{\alpha}}^D_{ex}(\omega) = \frac{e^2}{\hbar} \sum_n f_n(\omega) \sum_{J_z,i;J'_z,i'} \mathbf{r}^*_{iJ_z} \mathbf{r}^T_{i'J'_z} a^{n*}_i a^{n*}_{i'} \times \langle F^{J_z,\nu}_{hk} | F^{\sigma}_{el} \rangle^* \langle F^{J'_z,\nu'}_{hk'} | F^{\sigma'}_{el'} \rangle, \tag{A9}$$

where i runs over all possible combinations $\{el, \sigma; hk, \nu\}$ and

$$f_n(\omega) = \left(\frac{E^n_{ex}}{\hbar\omega}\right)\left[\frac{1}{E^n_{ex} - \omega - i\Gamma_n}\right].$$

The dynamic polarizability $\overleftrightarrow{\boldsymbol{\alpha}}^D_{ex}(\omega)$ can be used in the procedure described in Sec. II instead of $\overleftrightarrow{\boldsymbol{\alpha}}^D(\omega)$ to compute the magneto-optical response of the system.[16,59,60]

Taking into consideration four lowest hole energy states $h1(2)\nu$ ($\nu = \Uparrow, \Downarrow$) and four lowest electronic states $e1(2)\sigma$ ($\sigma = \uparrow, \downarrow$) (as it is described in Sec. III) the exciton Hamiltonian was numerically diagonalized after calculation of all involved matrix elements of the Green's function [Eq. (A6)]. Using the procedure described in Sec. II and parameters from Sec. III the ellipsometric angles of a layer of the asymmetric QDMs with accounting of possible excitonic effects were simulated.

To keep the paper within certain size limits we confine ourselves in this Appendix only to $\{d_1; \mathbf{B}_{[1]}\}$ and $\{d_3; \mathbf{B}_{[3]}\}$ configurations.[61] In Figs. 12 and 13 we show results of our simulations. Comparing Figs. 12(a) and 12(b) with Figs. 9(a) and 9(b) one can see that the most important difference is the obvious excitonic shift of the peak's positions (down by the energy axis) and some change (scaling) in the position of the crossing point: $B^{ex}_{1C} < B_{1C}$. The crossing itself is still a result of the nonuniform diamagnetic shifts for the energies of the excitons located in the large and small dot. This is a direct and clear consequence of the nonuniform diamagnetic shifts of the energies of noninteracting particles discussed in Sec. III. Before the crossing the exciton in the ground state is formed by the electron and hole located in the large dot, and after the crossing the electron and hole are both in the small dot. The change in B_{1C} is due to the difference in the values

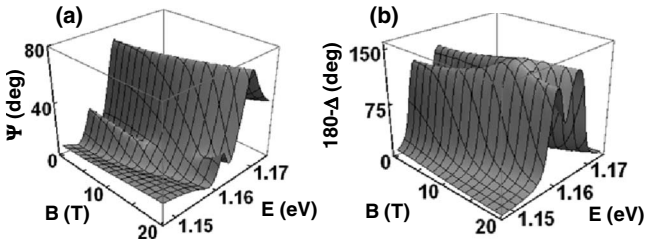

FIG. 12. Ellipsometric angles of the layer of QDM for $d=d_1$ and $\mathbf{B}=\mathbf{B}_{[1]}$ with possible excitonic effects included ($\hbar\Gamma=1$ meV).

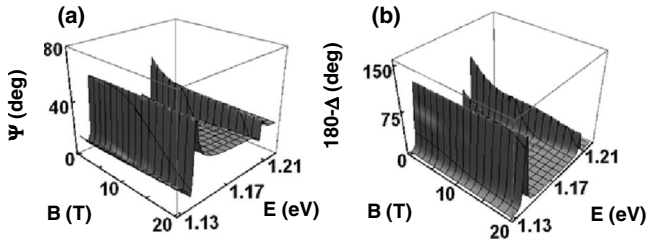

FIG. 13. Ellipsometric angles of the layer of QDM for $d=d_3$ and $\mathbf{B}=\mathbf{B}_{[3]}$ with possible excitonic effects included ($\hbar\Gamma=1$ meV).

of the excitonic binding energies for the excitons formed by the particles located in the large dot or small dot. For $\{d_3;B_{[3]}\}$ configuration the excitonic effects play a routine role: the main difference between Figs. 13(a) and 13(b) with Figs. 11(e) and 11(f) is just the overall excitonic shift of the peak's positions down by the energy axis.[3,8,9,12,13,57] We can conclude that the ellipsometric angles still reproduce changes in quantum-mechanical states of individual QDMs (now bound into excitons). For our asymmetrical QDM the ellipsometry data simulated with excitonic effects obviously resemble the data simulated without excitonic effects. Possible excitonic effects always can be accounted like it was described in this Appendix.

*Corresponding author; vam@faculty.nctu.edu.tw

[1] Z. R. Wasilewski, S. Farad, and J. P. McCaffrey, J. Cryst. Growth **201-202**, 1131 (1999).
[2] M. Bayer, P. Hawrylak, K. Hinzer, S. Farad, M. Korkusinski, Z. R. Wasilewski, O. Stern, and A. Forchel, Science **291**, 451 (2001).
[3] S. Taddei, M. Colocci, A. Vinattieri, F. Bogani, S. Franchi, P. Frigeri, L. Lazzarini, and G. Salviati, Phys. Rev. B **62**, 10220 (2000).
[4] B. D. Gerardot, I. Shtrichman, D. Hebert, and P. M. Petroff, J. Cryst. Growth **252**, 44 (2003).
[5] C. Kammerer, S. Sauvage, G. Fishman, P. Boucaud, G. Patriarche, and A. Lemaître, Appl. Phys. Lett. **87**, 173113 (2005).
[6] J. H. Oh, K. J. Chang, G. Ihm, and S. J. Lee, Phys. Rev. B **53**, R13264 (1996).
[7] H. Imamura, P. A. Maksym, and H. Aoki, Phys. Rev. B **59**, 5817 (1999).
[8] B. Szafran, S. Bednarek, and J. Adamowski, Phys. Rev. B **64**, 125301 (2001).
[9] Y. B. Lyanda-Geller, T. L. Reinecke, and M. Bayer, Phys. Rev. B **69**, 161308(R) (2004).
[10] G. Ortner, I. Yugova, G. Baldassarri Höger von Högersthal, A. Larionov, H. Kurtze, D. R. Yakovlev, M. Bayer, S. Fafard, Z. Wasilewski, P. Hawrylak, Y. B. Lyanda-Geller, T. L. Reinecke, A. Babinski, M. Potemski, V. B. Timofeev, and A. Forchel, Phys. Rev. B **71**, 125335 (2005).
[11] V. Mlinar, M. Tadić, and F. M. Peeters, Phys. Rev. B **73**, 235336 (2006).
[12] Q.-R. Dong, S.-S. Li, Z.-C. Niu, and S.-L. Feng, Physica E (Amsterdam) **33**, 230 (2006).
[13] J.-L. Zhu, W. Chu, Z. Dai, and D. Xu, Phys. Rev. B **72**, 165346 (2005).
[14] J. I. Climente, M. Korkusinski, G. Goldoni, and P. Hawrylak, Phys. Rev. B **78**, 115323 (2008).
[15] M. F. Doty, J. I. Climente, M. Korkusinski, M. Scheibner, A. S. Bracker, P. Hawrylak, and D. Gammon, Phys. Rev. Lett. **102**, 047401 (2009).
[16] O. Voskoboynikov, C. M. J. Wijers, J. L. Liu, and C. P. Lee, Phys. Rev. B **71**, 245332 (2005).
[17] V. G. Veselago, Sov. Phys. Usp. **10**, 509 (1968).
[18] S. A. Ramakrishna, Rep. Prog. Phys. **68**, 449 (2005).
[19] K. Asakawa, Y. Sugimoto, Y. Watanabe, N. Ozaki, A. Mizutani, Y. Takata, Y. Kitagawa, H. Ishikawa, N. Ikeda, K. Awazu, X. Wang, A. Watanabe, S. Nakamura, S. Ohkouchi, K. Inoue, M. Kristensen, O. Sigmund, P. I. Bogel, and R. Baets, New J. Phys. **8**, 208 (2006).
[20] D. R. Smith, J. B. Pendry, and M. C. K. Wiltshire, Science **305**, 788 (2004).
[21] W. J. Padilla, D. N. Basov, and D. R. Smith, Mater. Today **9**, 28 (2006).
[22] V. M. Agranovich and N. Gartstein Yu, Phys. Usp. **49**, 1029 (2006).
[23] V. M. Shalaev, Nat. Photonics **1**, 41 (2007).
[24] C. M. J. Wijers, J. H. Chu, J. L. Liu, and O. Voskoboynikov, Phys. Rev. B **74**, 035323 (2006).
[25] C. M. J. Wijers, J. H. Chu, and O. Voskoboynikov, Eur. Phys. J. B **54**, 225 (2006).
[26] O. Voskoboynikov, Phys. Rev. B **78**, 113310 (2008).
[27] M. A. Yurkin and A. G. Hoekstra, J. Quant. Spectrosc. Radiat. Transf. **106**, 558 (2007).
[28] B. T. Draine and Piotr J. Flatau, J. Opt. Soc. Am. A Opt. Image Sci. Vis **25**, 2693 (2008).
[29] C. M. J. Wijers, Phys. Rev. A **70**, 063807 (2004).
[30] J. Vlieger, Physica (Amsterdam) **64**, 63 (1973).
[31] C. M. J. Wijers and K. M. E. Emmett, Phys. Scr. **38**, 435 (1988).
[32] Yu. A. Il'inskii and L. V. Keldysh, *Electromagnetic Response of Material Media* (Plenum, New York, 1994).
[33] F. Thiele, Ch. Fuchs, and R. v. Baltz, Phys. Rev. B **64**, 205309 (2001).
[34] G. Ya. Slepyan, S. A. Maksimenko, V. P. Kalosha, A. Hoffmann, and D. Bimberg, Phys. Rev. B **64**, 125326 (2001).
[35] J. Avelin, Ph. D. thesis, Helsinki University of Technology, 2003.

[36] A. Sihvola, P. Ylä-Oijala, S. Järvenpää, and J. Avelin, IEEE Trans. Antennas Propag. **52**, 2226 (2004).
[37] P. G. Eliseev, H. Li, A. Stintz, G. T. Liu, T. C. Newell, K. J. Malloy, and L. F. Lester, Appl. Phys. Lett. **77**, 262 (2000).
[38] G. Bastard, *Wave Mechanics Applied to Semiconductor Heterostructures* (Les Edition de Physique, Les Ulis, 1990).
[39] O. Voskoboynikov, Yiming Li, Hsiao-Mei Lu, Cheng-Feng Shih, and C. P. Lee, Phys. Rev. B **66**, 155306 (2002).
[40] J. I. Climente, J. Planelles, and W. Jaskólski, Phys. Rev. B **68**, 075307 (2003).
[41] J. Planelles and W. Jaskólski, J. Phys.: Condens. Matter **15**, L67 (2003).
[42] S. L. Chuang, *Physics of Optoelectronic Devices* (Wiley, New York, 1995).
[43] H. Jiang and J. Singh, Phys. Rev. B **56**, 4696 (1997).
[44] C. Pryor, Phys. Rev. B **57**, 7190 (1998).
[45] O. Stier, M. Grundmann, and D. Bimberg, Phys. Rev. B **59**, 5688 (1999).
[46] J. I. Climente, J. Planelles, M. Pi, and F. Malet, Phys. Rev. B **72**, 233305 (2005).
[47] J. M. Luttinger and W. Kohn, Phys. Rev. **97**, 869 (1955).
[48] L. C. Andreani, A. Pasquarello, and F. Bassani, Phys. Rev. B **36**, 5887 (1987).
[49] L. G. C. Rego, P. Hawrylak, J. A. Brum, and A. Wojs, Phys. Rev. B **55**, 15694 (1997).
[50] I. Vurgaftman, J. R. Meyer, and L. R. Ram-Mohan, J. Appl. Phys. **89**, 5815 (2001).
[51] C. E. Pryor and M. E. Pistol, Phys. Rev. B **72**, 205311 (2005).
[52] www.comsol.com
[53] Y. Li, O. Voskoboynikov, C. P. Lee, S. M. Sze, and O. Tretyak, J. Appl. Phys. **90**, 6416 (2001).
[54] Terms with $|\langle F_{hk}^{+3/2,\Uparrow}|F_{el}^{\uparrow}\rangle|^2$ and $|\langle F_{hk}^{-3/2,\Downarrow}|F_{el}^{\downarrow}\rangle|^2$ give about equivalent contributions to the dynamic part of the polarizability but they present optical transitions with different configurations of chirality and spin.
[55] T. Le Minh and O. Voskoboynikov, Phys. Status Solidi B **246**, 771 (2009).
[56] *Handbook of Ellipsometry*, edited by H. Tompkins and E. A. Irene, (William Andrew, New York, 2005).
[57] J. Li and J.-B. Xia, Phys. Rev. B **61**, 15880 (2000).
[58] K. L. Janssens, F. M. Peeters, and V. A. Schweigert, Phys. Rev. B **63**, 205311 (2001).
[59] E. L. Ivchenko, Y. Fu, and M. Willander, Phys. Solid State **42**, 1756 (2000).
[60] Y. Fu, H. Ågren, L. Höglund, J. Y. Andersson, C. Asplund, M. Qiu, and L. Thylén, Appl. Phys. Lett. **93**, 183117 (2008).
[61] A complete description of the magnetoexcitonic properties of the system will be presented somewhere else.